Article

A Comparison of Chitosan Adhesion to KOH and H$_2$O$_2$ Pre-Treated Electrospun Poly(3-Hydroxybutyrate) Nanofibers

Yansheng Zhou [1], Daqing Li [2], Xin Li [3], Ying Li [2], Bing Li [1,*] and Fenglei Zhou [4,5,*]

1   Institute for Materials Discovery, Faculty of Mathematical Physical Sciences, University College London, Malet Place, London WC1E 7JE, UK; yansheng.zhou.19@ucl.ac.uk
2   Spinal Repair Unit, Department of Brain Repair and Rehabilitation, Institute of Neurology, University College London, Queen Square, London WC1N 3BG, UK; daqing.li@ucl.ac.uk (D.L.); ying.li@ucl.ac.uk (Y.L.)
3   School of Finance & Accounting, University of Westminster, London NW1 5LS, UK; x.li1@westminster.ac.uk
4   Centre for Medical Image Computing, Department of Medical Physics and Biomedical Engineering, University College London, London WC1V 6LJ, UK
5   College of Textiles and Clothing, Qingdao University, Qingdao 266071, China
*   Correspondence: bing.li@ucl.ac.uk (B.L.); fenglei.zhou@ucl.ac.uk (F.Z.)

Abstract: Chitosan coatings could effectively increase the biostability and biocompatibility of biomaterials while maintaining their structural integrity. In this study, electrospun fibrous polyhydroxybutyrate (PHB) membranes were pre-treated with potassium hydroxide (KOH) or hydrogen peroxide (H$_2$O$_2$) and then modified with dopamine (DA) and glutaraldehyde (GA) to improve their adhesion with chitosan (CS). Scanning electron microscopy (SEM), water contact angles (WCA), and Fourier transform infrared spectroscopy (FTIR) were used to demonstrate the successful generation of DA and GA-modified PHB fibers. KOH pre-treated PHB membranes exhibited superior binding efficiency with CS at low concentrations compared to their H$_2$O$_2$ pre-treated counterparts. The thermal analysis demonstrated a considerable decrease in the degradation temperature and crystallinity of KOH pre-treated membranes, with temperatures dropping from 309 °C to 265.5 °C and crystallinity reducing from 100% to 25.59% as CS concentration increased from 0 to 2 w/v%. In comparison, H$_2$O$_2$ pre-treated membranes experienced a mild reduction in degradation temperature, from 309 °C to 284.4 °C, and a large decrease in crystallinity from 100% to 43%. UV-vis analysis using Cibacron Brilliant Red 3B-A dye (CBR) indicated similar binding efficiencies at low CS concentrations for both pre-treatments, but decreased stability at higher concentrations for KOH pre-treated membranes. Mechanical testing revealed a considerable increase in Young's modulus (2 to 14%), toughness (31 to 60%), and ultimate tensile stress (UTS) (14 to 63%) for KOH-treated membranes compared with H$_2$O$_2$ pre-treated membranes as CS concentration increased from 0 to 2 w/v%.

Keywords: polyhydroxybutyrate–chitosan composite nanofibers; alkaline surface modification; electrospinning; CBR analysis

1. Introduction

Poly(3-hydroxybutyrate) (PHB) is a biodegradable polymer that can be extracted from microbial intracellular contents and degraded under ambient conditions [1]. PHB, compared to other natural polymers like chitosan, collagen, and elastin, has better biodegradability, biocompatibility, nontoxicity, structural stability, and mechanical properties that can be used to support hard tissue for long-term regeneration, e.g., bone and nerve regeneration [2,3]. Recently, with the developments of advanced fabrication techniques, PHB has been used for soft tissue applications, such as cartilage [4], nerve [5], skin [6], and blood vessels [7]. However, PHB is often limited by its hydrophobicity due to the methyl functional group (CH$_3$) and an ester linkage group (−COOR) presented along its side chain. This hydrophobicity has constrained cells or bioactive molecules' binding affinity, which has limited its potential in tissue engineering applications [5]. Hence, surface functionalization

of PHB is an essential process to alter its chemical characteristics and increase its surface activity and bioactivity.

Different surface functionalization methods have been widely reported to overcome these drawbacks of electrospun PHB fibers. In general, these methods can be classified into chemical and physical approaches. In chemical approaches, monomer grafting techniques could highly alter electrospun PHB fibers to be hydrophilic and cytocompatible. For example, polydopamine (PDA), due to the coexistence of the catechol and amine groups of dopamine, could improve its adhesion to various materials, allowing secondary reactions with biomolecules and thiolated groups [8]. However, chemical surface treatment is costly and time-consuming. Moreover, polydopamine or ammonolysis by ethylenediamine may affect the physical properties of the electrospun fiber. The former requires alkali pre-treatment by dipping the substrates in alkaline dopamine solutions (e.g., pH 8.5) and causes a reduction of crystallinity [9], and the latter causes erosion after a long treatment time. In physical surface modification, plasma treatment is largely a non-specific method that is used in different polymer systems to improve surface properties [8]. The plasma treatments, such as oxygen, air, argon, and nitrogen, introduce higher-oxidation-state carbon species with hydroxy, ether, and carbonyl groups [8–10]. However, these surface functionalization techniques often suffer from a lack of coating or treatment homogeneity and have limited penetration depth through the fibrous membrane. Blends, emulsions, and composites offer versatile approaches to material fabrication, allowing precise thickness control and eliminating the need for solvents. For instance, core-shell electrospun fiber structures can be employed as drug delivery systems to significantly mitigate the initial burst of drug release, resulting in a more controlled release profile [10]. Moreover, by optimizing the composition and structure of composites, it is possible to counterbalance individual drawbacks in various properties. Examples include enhancing mechanical properties such as tensile strength and flexibility, improving thermal properties like thermal stability and heat resistance, increasing chemical stability against degradation, and ensuring compatibility between different material components for better interfacial bonding [11]. Thus, a well-designed composite material can exhibit improved overall performance in diverse applications.

Chitosan (CS) is a natural polysaccharide produced through the deacetylation of chitin that originates from the external skeleton of different insects and crustaceans. Chitosan has recently been used as a type of biomaterial for tissue engineering because of its good biocompatibility, biodegradability, anti-bacterial properties, and low cost. Due to its cation present in the solution, it could naturally attract anion proteins or growth factors such as nerve growth factors [12]. According to our previous research, blending chitosan with PHB will alter its hydrophobicity to hydrophilicity, becoming more anti-bacterial, biodegradable, and biocompatible with cells and tissues [9,13]. Furthermore, chitosan in the blended material provides many primary amino groups for further modifications such as biomolecule conjugation and thus diversifies the possible applications of this blended material. However, blended PHB and CS will cause phase separation with improper compositions [9] and limit its applications. Additionally, our previous reports have indicated that blending CS with PHB will decrease its thermal and structural stability in both acidic and alkaline PBS solutions [9].

Electrospinning and electrospun membranes have been extensively used to fabricate polymeric nanofibers, which highly monitor extracellular matrix (ECM)-mimicking structures [2,4,8,9]. Electrospun materials have several advantages, including extremely large specific surface areas, wide size ranges from the nanometer to micrometer, high porosity, and superior mechanical properties. Synthetic polymers such as polycaprolactone (PCL) [14], poly(lactic-co-glycolic acid) (PLGA) [15], and poly(3-hydroxybutyrate) (PHB) have been electrospun into nanofibers for biomedical applications including peripheral nerve scaffolds. However, the degradation patterns of common bio polyesters, such as PLA, PGA, PCL, and their copolymers, will increase the pH values of body fluid around injured sites and elevate its oxidative stress, which could cause secondary injuries [16]. PHB materials, on the other hand, are good candidates for use in tissue regeneration because they do not produce obvious acidic byproducts.

Although several studies on dopamine surface-treated PHB/chitosan electrospun fiber (PHB-DA-CS) films have been investigated extensively in the literature, few studies have mentioned the influences of CS binding efficiency on PHB electrospun fibers following KOH and H_2O_2 pre-treatment. Examining potassium hydroxide (KOH) and sodium hydroxide reveals KOH's slight molecular advantage, allowing it to cut through oil molecules more rapidly [14,17–20]. Additionally, the robust alkaline nature of KOH facilitates vigorous surface oxidization, even at low concentrations [17]. This is particularly advantageous for preventing the alkaline degradation of PHB electrospun fibers, highlighting the importance of understanding and leveraging KOH's unique properties. Previous studies have shown that the persistence of the H_2O_2 used as a surface oxidant on PCL polymers gradually decreases after 2–3 weeks [8,21–23]. Additionally, there is a lack of studies about the physical, chemical, and mechanical characterization of the PHB-DA-CS nanofibrous membranes with different concentrations of CS. Therefore, the aim of this proposed research is the study of the variations in physical and chemical properties of PHB polymers with different H_2O_2 and KOH surface oxidants and their CS binding efficiencies.

2. Materials and Methods

2.1. Materials

Polyhydroxybutyrate (PHB, Mw $\approx$ 660,000 g/mol) was purchased from Merck (London, UK) and Chitosan (CS, medium Mw) was purchased from Sigma-Aldrich in St. Louis, MO, USA. A 50 v/v% H_2O_2 solution was purchased from Sigma-Aldrich, St. Louis, MO, USA, KOH > 99% was purchased from Sigma-Aldrich, Dopamine-HCl was purchased from Merck, Tris-HCl was purchased from Sigma-Aldrich, St. Louis, MO, USA, glutaraldehyde solution (GA, 50 wt. % in H_2O) was purchased from Merck, acetic acid (>99% grade) was purchased from Merck, chloroform (>99.8% grade) was purchased from Sigma-Aldrich, and N,N-Dimethylformamide (DMF) (anhydrous, >99.8% grade) was purchased from Sigma-Aldrich.

2.2. Preparing PHB and CS Solutions

The concentration of PHB/CS solutions with different surface treatment was shown in Table 1. PHB solution was prepared by adding 1.5 g of PHB pellets to 10 mL of chloroform/DMF (9:1 v/v) to form a 15 w/v% polymer solution and stirring under reflux at 100 °C for 3 h until a homogenous solution formed. A 2 w/v% CS solution was prepared by adding 0.2 g of CS powder into an acetic acid/water mixing solution (1:9 v/v) and stirring at room temperature for 24 h until homogenous. Furthermore, 0.2, 0.5, 0.8, 1, and 1.5 w/v% CS solutions were prepared through serial dilution of 2 w/v% CS solution. All the solutions were stored at room temperature and sealed with Parafilm until further use.

Table 1. Surface treatment and concentration of CS in PHB samples.

Sample Name	Concentration of PHB (w/v%)	Concentration of CS (w/v%)	Reagent for Surface Treatment
PHB-H-0-CS	15	0	
PHB-H-0.2-CS	15	0.2	
PHB-H-0.5-CS	15	0.5	
PHB-H-0.8-CS	15	0.8	H_2O_2
PHB-H-1-CS	15	1	
PHB-H-1.5-CS	15	1.5	
PHB-H-2-CS	15	2	
PHB-K-0-CS	15	0	
PHB-K-0.2-CS	15	0.2	
PHB-K-0.5-CS	15	0.5	
PHB-K-0.8-CS	15	0.8	KOH
PHB-K-1-CS	15	1	
PHB-K-1.5-CS	15	1.5	
PHB-K-2-CS	15	2	

2.3. Fabrication of PHB Electrospun Fibers

Randomly oriented microfibers were fabricated via single-jet electrospinning. 15 wt% PHB solutions were placed in a 5 mL thermos syringe with an 18-gauge needle. Based on the operation diagrams of the PHB/CF/DMF solution system, the process parameters were set as follows: a flow rate of 2 mL/h and an electric field strength of 0.5 kV/cm, which was the ratio between the applied voltages (AV) and working distance (WD). The electrospun PHB membranes were collected in foil at room temperature with 25% relative humidity and washed with ethanol/deionized water after fabrication 3 times; this helped remove extra CF and DMF present in the samples.

2.4. Surface Functionalization of Electrospun Fibrous PHB Membranes with DA and GA

As shown in Figure 1, 2 cm × 2 cm × 0.01 cm sections of the PHB electrospun membranes were further cut and treated in 0.5 M KOH (pH = 12.5) and 50 v/v% H_2O_2 (pH = 5.5) solutions for 1 h at room temperature, followed by washing with deionized water three times. Following that, the PHB fiber membranes were submerged in a 3 mg mL1 dopamine/0.1 M Tris buffer solution at pH 8.5 and 60 °C for 24 h in the dark. Following the completion of the anchoring reaction, the PHB–dopamine (PHB-DA) membranes were washed several times with deionized water. Furthermore, the membranes were submerged in a 3% glutaraldehyde (GA) aqueous solution for 6 h, forming PHB-DA-GA membranes. In this system, glutaraldehyde served as a coupling agent by providing reactive aldehyde groups for covalent interactions between dopamine and chitosan. The unattached GA was washed away using deionized water. Then, we added CS to the dish containing the PHB-DA-GA membranes. The CS was added in concentrations of 0.2, 0.5, 0.8, 1, 1.5, and 2 weight/volume percent, and we used 2 mL of it each time. The dish was then set aside for 24 h at room temperature, allowing the membranes to be coated by the CS. During this stage, imine bonds were generated between the aldehyde groups on the membrane surface and the main amino groups at the C-2 locations of the chitosan, and the GA-treated PHB-DA membrane substrates were submerged in the chitosan solution for 24 h. Before conducting the studies, the produced PHB-KOH-DA-GA-0.2/0.5/0.8/1/1.5/2 w/v% CS(PHB-K-0.2-CS, PHB-K-0.5-CS, PHB-K-0.8-CS, PHB-K-1-CS, PHB-K-1.5-CS, and PHB-K-2-CS) and PHB-H_2O_2-DA-GA-0.2/0.5/0.8/1/1.5/2 w/v% CS (PHB-H-0.2-CS, PHB-H-0.5-CS, PHB-H-0.8-CS, PHB-H-1-CS, PHB-H-1.5-CS, and PHB-H-2-CS) substrates were washed with deionized water to eliminate unattached polymers. The substrates were then cleaned with deionized water and vacuum-dried overnight at room temperature for further characterization.
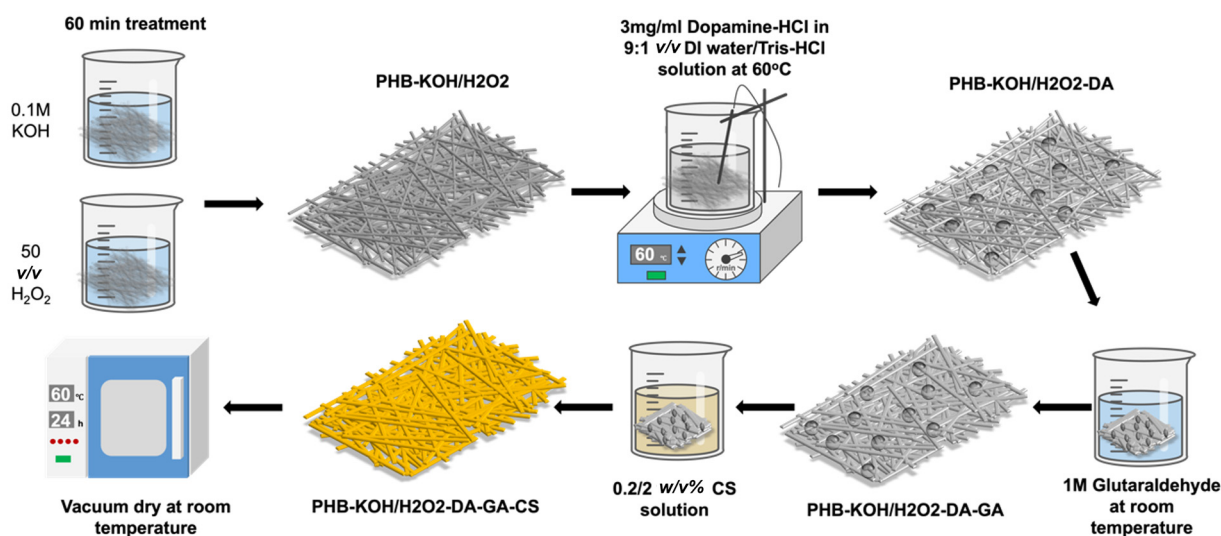

Figure 1. Schematics of the PHB-DA-GA-CS electrospun fiber modification process.

2.5. Scanning Electron Microscopy (SEM)

The PHB nanofibers were examined utilizing a Hitachi 8230 field emission SEM. To enhance conductivity and visibility, the specimens were sputtering coated with a 20 nm thick layer of gold. ImageJ 1.52 was used to determine the diameters of the fibers. One hundred measurements were conducted for each individual sample.

2.6. Attenuated Total Reflection-Fourier Transform Infrared Spectroscopy (ATR-FTIR)

To explore the functional groups on the electrospun PHB/CS nanofibers, ATR-FTIR was employed. Prior to the analysis, the fibers underwent a thorough rinse with deionized water and were subsequently dried in a vacuum dryer. The spectra were acquired during a 5 min scan from 4000 cm^{-1} to 400 cm^{-1}, with a step size of 2.0 cm^{-1}.

2.7. Thermalgravimetric Analysis (TGA)

The electrospun PHB fibers were tested using a PerkinElmer 2000 TGA system with a nitrogen flow rate of 40 mL/min. A 10 mg sample was carefully prepared and subsequently heated from 50–400 °C, employing a heating rate of 10 °C/min.

2.8. Differential Scanning Calorimetry (DSC)

DSC analysis was conducted by placing 2 mg samples into an aluminum crucible, which was then heated up from 25 to 550 °C at 10 °C/min. The nitrogen flow was kept at 20 mL/min. To ensure consistency and comparability, all the samples were analyzed under identical conditions to generate the TGA results.

2.9. Contact Angle Analysis

To assess the wettability of the fiber mats, an OCA 15 plus sessile drop water system was used to measure the contact angle. This system was equipped with a CCD camera with a precision of ±0.2°. All the measurements were carried out at room temperature, and ultra-pure water was used for the tests. To obtain reliable results, each specimen underwent five repetitions, with each specimen generating 50 data points. The average values were subsequently calculated based on these measurements.

2.10. BET Analysis of Porosity

A NOVA Touch (Quantachrome Instruments, London, UK) was used to measure the porosities of the samples in this project. To prepare the samples, they were first vacuum-dried at room temperature for 24 h and weighed. Nitrogen gas was used as the adsorbate in the BET test at 77.35 K. A 600 s thermal delay was used, together with helium backfill mode. The adsorption isotherm curve was used to calculate the specific surface area of the monoliths, while density-functional theory (DFT) was used to model the distribution of half-pore widths.

2.11. Stability Analysis of CS on KOH and H_2O_2-Treated PHB-DA-GA-CS Electrospun Fibers

To analyze the binding efficiency of chitosan, Cibacron Brilliant Red 3B-A dye (CBR) was used to measure the chitosan concentration remaining in the solution. Firstly, each sample was immersed in PBS in solution (PBS/CS) at room temperature for 14 days. On days 1, 3, 7, and 14, 1 mL of the PBS/CS solution was collected and ready for use. Secondly, 0.075 g of Cibacron Brilliant Red 3B-A powder (50% dye content) was dissolved in 0.5 L of DI water to form 0.075 M dye solutions. The PBS/CS solutions were added to glass tubes containing 0.1 mL of buffer glycine/HCl and 1 mL of dye. Thirdly, the final volume was diluted to 5 mL using DI water. The tubes were sealed and kept at room temperature under continuous agitation. After 20 min, 1 mL from each tube was transferred to a tube, and the measuring absorption relative to DW was measured using the same spectrophotometer. The BR absorption spectrum exhibited a broad peak with a plateau between 506 and 550 nm in UV-vis. The actual amount of CS in 0.2, 0.5, 0.8, 1, 1.5, and 2 *w/v*% concentrations was first determined using UV-vis at a wavelength of 530 nm. These wavelength values correspond

to the maximum wavelength for each concentration of CS. The results were reported as the averages of at least five measurements.

2.12. Mechanical Tests

Mechanical tests were performed using an Intron tensile tester according to the active standard test method D638 equipped with a 50 N static load cell. During the test, the samples were cut into 10 mm $\times$ 10 mm square films with a thickness of 0.5 ± 0.02 mm. Furthermore, the tensile strength and elongation were calculated at the point of fracture based on the measured thickness and width of each sample. A test speed of 10 mm min^{-1} was used. For each measurement within each batch, we meticulously prepared 5 to 10 individual samples. Subsequently, we conducted measurements on all of these samples to ensure that we consistently obtained a minimum of 5 data points for each specific analysis. This rigorous approach ensured the reliability and robustness of the data for further analysis.

2.13. Statistical Analysis

The significant difference analyses in the above sections were analyzed using one-way ANOVA tests in Prism 8. Statistically significant differences were considered at a *p* values less than 0.05.

3. Results and Discussion

3.1. Morphology and Size of Electrospun Membranes with Varying CS Concentrations (0.2–2 w/v%) in PHB-KOH/H_2O_2

The morphology and diameters of the electrospun PHB fibers after a series of chemical post-treatments are shown in Figures 2 and 3. The untreated PHB electrospun fibers exhibited diameters of 5.22 ± 0.047 μm. After the KOH and H_2O_2 treatments, the fiber diameters decreased to 1.90 ± 0.42 μm and 2.78 ± 0.12 μm, respectively, due to the hydrolysis caused by the KOH treatment and the peroxide radicals grafted on the PHB surface during the H_2O_2 treatment. Furthermore, Figure 2 reveals small islets of DA on the surfaces of both the KOH and H_2O_2-treated fibers resulting from surface oxidation and roughness changes. In a comparative analysis between potassium hydroxide (KOH) and sodium hydroxide, it becomes evident that the former's molecular size is slightly smaller. This attribute of potassium hydroxide allows it to interact with PHB more swiftly, ultimately enhancing its hydrophilicity. Furthermore, the compelling alkaline properties of potassium hydroxide (KOH) offer significant benefits. These properties tend to induce surface oxidization with more intensity, even in low concentrations, which is a crucial aspect of its applications.

Figure 2 and Table 2 displays the fiber diameters and images of KOH and H_2O_2-treated PHB-DA-GA-CS with varying CS concentrations. The mean fiber diameters of the PHB-DA-GA-CS membranes exhibited a significant increase from 1.90 to 3.14 μm and between 0.2 *w/v*% and 2 *w/v*% CS (from 2.90 to 4.44 μm). At a 0.8 *w/v*% CS concentration, both the KOH and H_2O_2-treated fibers showed a thin layer attached to the fibrous membrane surface. The KOH-treated fibers displayed a higher increment in fiber diameter than the H_2O_2-treated fibers between 0.2 *w/v*% and 2 *w/v*% CS concentrations due to more effective oxidation of the KOH pre-treatment, providing increased anchor sites for dopamine and CS on the fiber surface.

Figures 2 and 3 also reveal that between 0.2 and 0.5 *w/v*% CS, both the KOH and H_2O_2 treatments result in evenly distributed CS coatings on individual PHB fibers. At CS concentrations of 0.8–1.5 *w/v*%, KOH-treated fibers exhibited a more uniform CS coating, while H_2O_2-treated fibers had the most CS forming between the fiber layers. At 2 *w/v*% CS, neither treatment achieved a uniform CS coating due to high viscosity, indicating that CS attaches more efficiently to KOH-treated PHB fibers compared to H_2O_2-treated fibers.
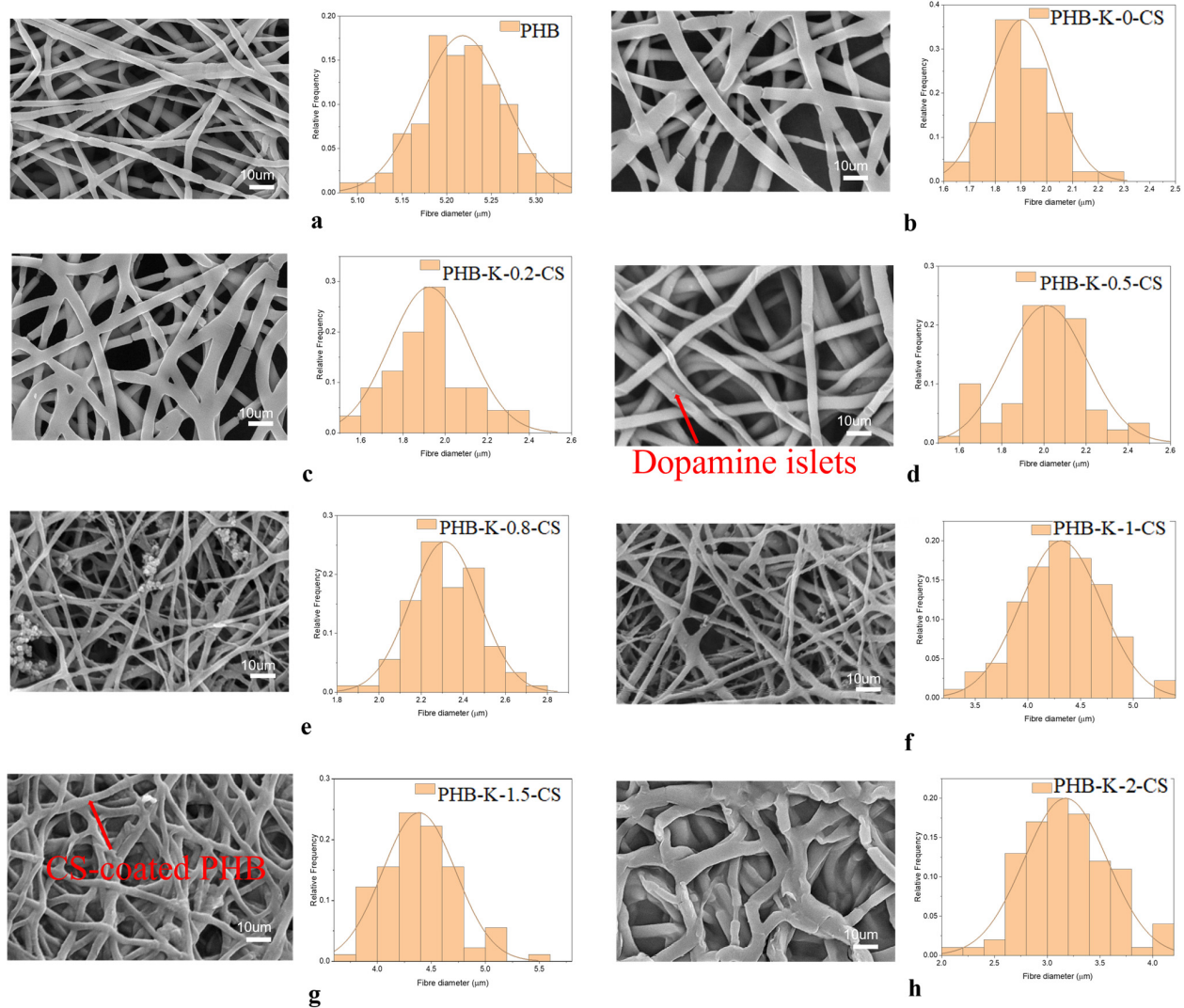
Figure 2. SEM micrographs and fiber diameters of PHB/KOH-treated electrospun fibers with varying chitosan concentrations: (**a**) non-treated PHB fibers, (**b**) 0 $w/v\%$, (**c**) 0.2 $w/v\%$, (**d**) 0.5 $w/v\%$, (**e**) 0.8 $w/v\%$, (**f**) 1 $w/v\%$, (**g**) 1.5 $w/v\%$, (**h**) 2 $w/v\%$.

Table 2. Average fiber diameters and standard deviations for PHB electrospun fibers subjected to KOH and H_2O_2 treatments with varying chitosan (CS) concentrations.

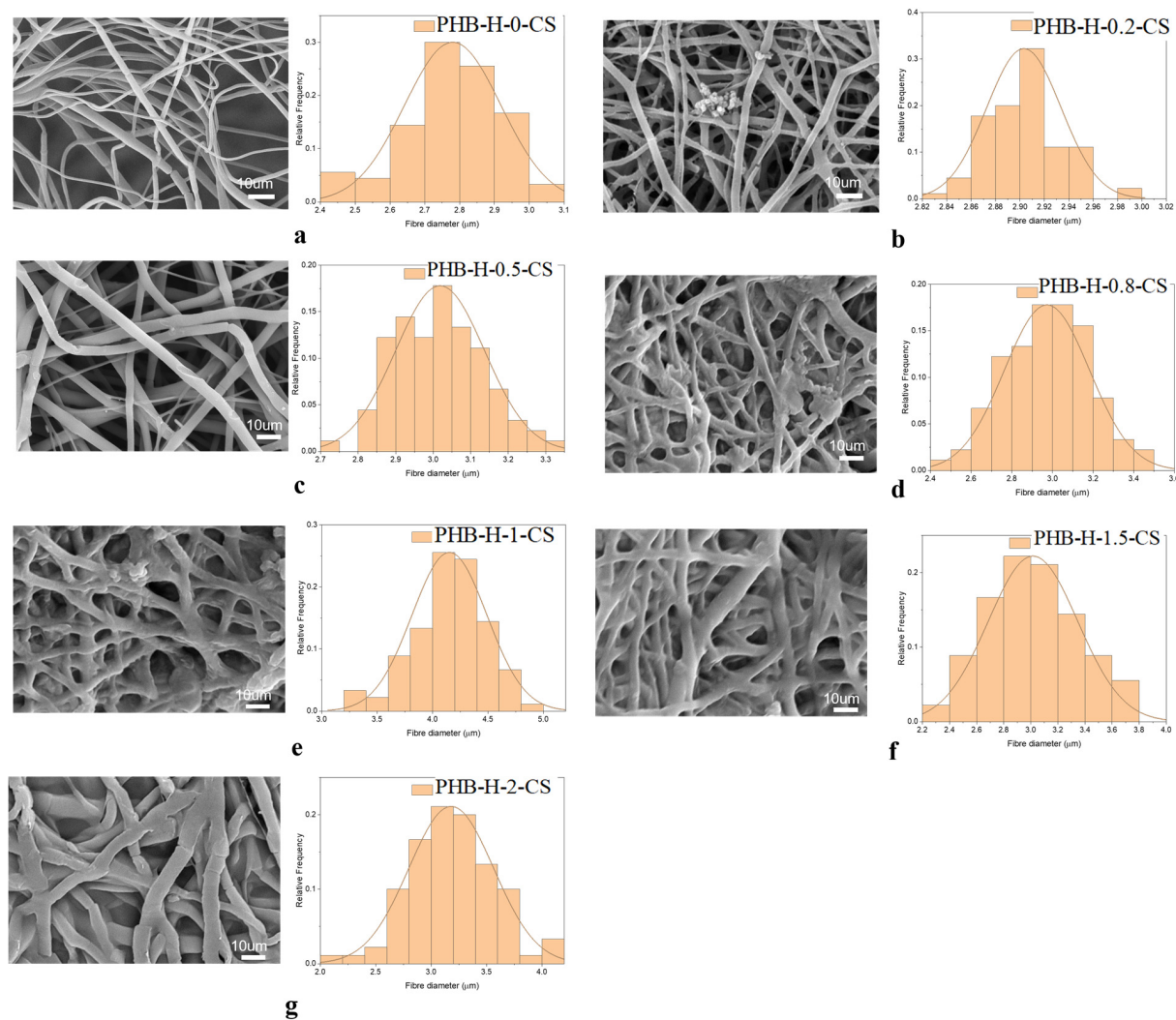| Groups	Fiber Diameter (µm)	Standard Deviation
PHB (non-treated)	5.22	0.05
PHB-H-0-CS	2.78	0.14
PHB-H-0.2-CS	2.90	0.03
PHB-H-0.5-CS	3.01	0.11
PHB-H-0.8-CS	3.00	0.20
PHB-H-1-CS	4.10	0.33
PHB-H-1.5-CS	4.32	0.37
PHB-H-2-CS	4.41	0.34
PHB-K-0-CS	1.90	0.12
PHB-K-0.2-CS	1.93	0.18
PHB-K-0.5-CS	1.98	0.19
PHB-K-0.8-CS	2.31	0.18
PHB-K-1-CS	2.78	0.31
PHB-K-1.5-CS	2.98	0.35
PHB-K-2-CS	3.14	0.42

Figure 3. SEM micrographs of PHB/H$_2$O$_2$-treated electrospun fibers with varying chitosan concentrations: (**a**) 0 *w/v*%, (**b**) 0.2 *w/v*%, (**c**) 0.5 *w/v*%, (**d**) 0.8 *w/v*%, (**e**) 1 *w/v*%, (**f**) 1.5 *w/v*%, (**g**) 2 *w/v*%.

3.2. Total Reflectance-Fourier Transform Infrared (ATR-FTIR)

Figure 4 displays the attenuated ATR-FTIR spectra of electrospun non-treated and treated PHB. The PHB exhibited unique peaks for C=O stretching, which were located close to 1725 cm^{-1}, and those for v(C-H) stretching were discovered between 2950 and 2820 cm^{-1}. Following KOH or H$_2$O$_2$ treatment, both PHB samples maintained their usual peaks and produced a bandwidth linked to -OH groups in the 3600–3200 cm^{-1} range, demonstrating the effective induction of hydrophilicity. Additionally, the spectrum after DA coating showed a broad peak at 3630–3120 cm^{-1} revealing the hydroxyl and catechol groups, and the peaks at 520 cm^{-1} and 2945 cm^{-1} were attributed to the stretching of aromatic C=C bonds in the indole and N-H amines. These are all characteristic peaks of DA, which have been proven in other studies [5,9,11]. These results confirm successful binding between PHB fibers and PDA. Both of these peaks were revealed in the PHB-DA-GA and PHB-DA-GA-CS spectra. Furthermore, the signals displayed a decrease due to the lower amount of hydroxyl groups, which also indicated PDA grafting on the PHB fibers.

In Figure 4c, the FTIR spectra of KOH/H$_2$O$_2$-treated PHB electrospun fibers after exposure to different concentrations of CS are displayed. It was found that KOH treatment resulted in higher signal amplification at peaks of 3415 cm^{-1} (-OH groups) and 1557 cm^{-1} (-NH3 groups) compared to H$_2$O$_2$. This can be explained by KOH inducing hydrolysis degradation of PHB, which could break the ester bonds and result in the formation of

a high number of -OH groups at the surface of PHB, whereas H_2O_2 performs a simple oxidation reaction with the ester, forming OH groups. These causes the KOH pre-treatment to be more effective in binding with other active sites of chemicals or proteins when other conditions are the same [24–26]. As a result, more DA and CS molecules were attached to the -OH binding site. In the KOH-treated PHB fibers, when increasing concentrations of CS were added, the signals in the fingerprint regions of 816–826 cm^{-1} and 1276–1278 cm^{-1} were weakened by the addition of CS, which indicates a reduction in the crystallinity of PHB. Meanwhile, the H_2O_2-treated PHB showed no differences in the fingerprint region, which showed minimal changes in crystallinity after the addition of CS. In addition, the N-H amine peaks at 3372 cm^{-1} and 1623 cm^{-1} were revealed at different concentrations of CS solution, as shown in Figure 4b,c. These results indicate that the KOH-treated PHB electrospun membranes were successfully bound to the PHB electrospun fibers in both high and low concentrations of CS, whereas the H_2O_2-treated membranes could bind CS in high concentrations.
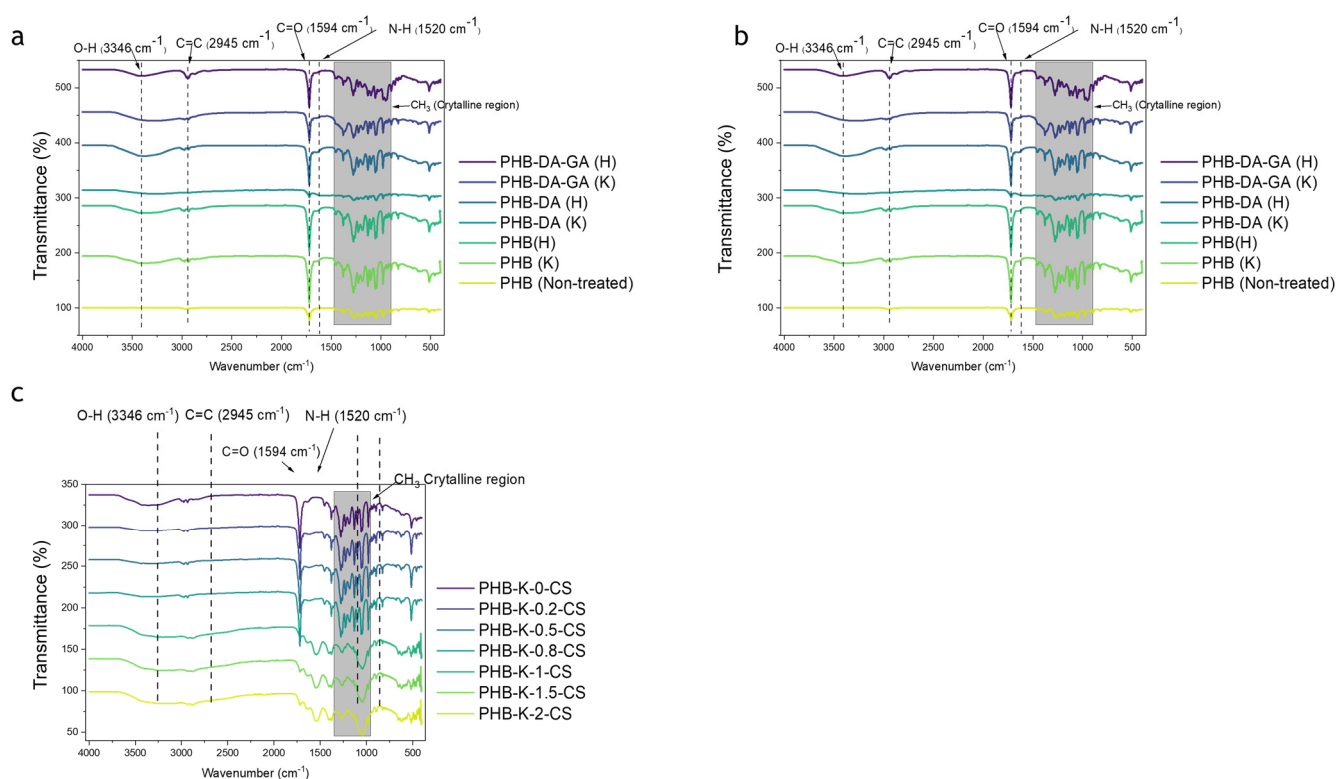

Figure 4. (**a**) FTIR spectra comparisons for PHB, PHB−DA, PHB−DA−GA, and PHB−DA−GA−CS (2 and 0.2 w/v%) with KOH (K) and H_2O_2 (H) treatments. (**b**) FTIR spectra of KOH−treated PHB−DA−GA−CS electrospun fibers with chitosan concentrations ranging from 0 to 2 w/v%. (**c**) FTIR spectra of H_2O_2-treated PHB−DA−GA−CS electrospun fibers with chitosan concentrations ranging from 0 to 2 w/v%.

3.3. TGA and DTA Analysis of PHB-CS Electrospun Fibers

The influence of H_2O_2/KOH surface modification while using varying CS concentrations on the structural properties of PHB electrospun fibers was thoroughly investigated through thermal analysis. Because our instruments occasionally encountered issues during thermal analysis when employing diverse techniques, and due to the extremely low weight of our polymer membrane samples, there was a tendency for them to be displaced during the thermal analysis process, potentially resulting in negative weight percentages. Nevertheless, it is important to note that all the data points in our study were consistently replicated and can be considered reasonably reliable. Utilizing techniques like TGA and DTA, the changes induced by these factors can be elucidated. The detailed results of these

examinations are depicted in Figure 5. Our findings indicate that all the samples demonstrated two distinct peaks at elevated temperatures in their heating curves. In Tables 3 and 4, the temperatures depicted in the first melting temperature (T_1) corresponded to either the amorphous region of PHB or the present CS contents, providing insights into their thermal characteristics. Conversely, the second melting temperature (T_2) represents the temperature at which the crystalline region of PHB undergoes degradation, highlighting the thermal stability of this specific region [20]. In Figure 5a–d, a comparable thermogram profile could be found in all the presented curves, showing significant changes compared to PHB. Corroborating prior research [9], T_1 and T_2 were between 250–300 °C and 340–390 °C [9,21]. This overlap validates the reliability of our findings. Upon applying the pre-treatment of H_2O_2/KOH to PHB along with dopamine (DA), there was a notable decrease in the T_1 and T_2 temperatures of the electrospun PHB fibers. Specifically, the T1 temperature dropped to 233.3 °C and 221.4 °C, while T2 descended to 348.2 °C and 344.6 °C, respectively. (Table 3). KOH, compared with H_2O_2, had a greater impact on the thermal stability of the electrospun PHB nanofibers. This is because the strong alkaline properties of KOH can reduce the crystallinity of PHB and damage its lamellar structure by hydrolyzing into carboxylic acid and alcohol in the base solution [9,22,23]. On the other hand, because KOH performed stronger surface oxidation than H_2O_2, KOH pre-treatment resulted in a stronger enhancement of the deposition of DA coating than H_2O_2 and protected the PHB fibers from breaking down upon heating. This can be proven by the initial stage breakdown (150–250 °C) of the KOH-DA coating (red curve), showing better thermal stability than the H_2O_2-DA coating. Furthermore, the lower weight loss of the KOH-DA-treated PHB fibers in the 300–400 °C range showed an increase in thermal stability to PHB after the breakdown of PDA. This reduction in weight loss can be explained by the increased affinity between the hydroxyl (-OH) groups, which was introduced onto the PHB fiber surface by the KOH treatment, and the amine and catechol moieties of dopamine (DA). This enhanced interaction results in higher surface adherence.

Table 3. TGA analysis for PHB-KOH treated electrospun nanofibers with 2, 1.5, 1, 0.8, 0.5, and 0.2 *w/v*% CS.

Temperature	First Melting Temperature (T_1)	Second Melting Temperature (T_2)	*p* Value (Compared to PHB-KOH-DA-GA-0 *w/v*% CS)
PHB-K-0-CS	113 ± 4.14	280 ± 13.2	/
PHB-K-0.2-CS	98.7 ± 5.43	290 ± 12.2	0.712
PHB-K-0.5-CS	93.7 ± 7.32	289 ± 6.62	0.691
PHB-K-0.8-CS	100 ± 6.12	285 ± 8.34	0.681
PHB-K-1-CS	102 ± 4.12	281 ± 7.12	<0.05
PHB-K-1.5-CS	88.8 ± 6.13	263 ± 5.12	<0.05
PHB-K-2-CS	92.9 ± 8.12	269 ± 5.32	<0.05

Table 4. TGA analysis for PHB-H_2O_2 treated electrospun nanofibers with 2, 1.5, 1, 0.8, 0.5, and 0.2 *w/v*% CS.

Temperature	First Melting Temperature (T_1)	Second Melting Temperature (T_2)	*p* Value (Compared to PHB-H_2O_2-DA-GA-0 *w/v*% CS)
PHB	309 ± 3.41	368 ± 5.12	<0.05
PHB-H-0-CS	110 ± 8.12	275 ± 11.1	/
PHB-H-0.2-CS	128 ± 5.123	282 ± 9.77	0.555
PHB-H-0.5-CS	128 ± 4.53	282 ± 6.99	0.781
PHB-H-0.8-CS	128 ± 6.21	282 ± 4.51	0.841
PHB-H-1-CS	128 ± 5.12	281 ± 6.34	0.813
PHB-H-1.5-CS	128 ± 3.53	282 ± 5.32	<0.05
PHB-H-2-CS	129 ± 5.12	284 ± 6.54	<0.05

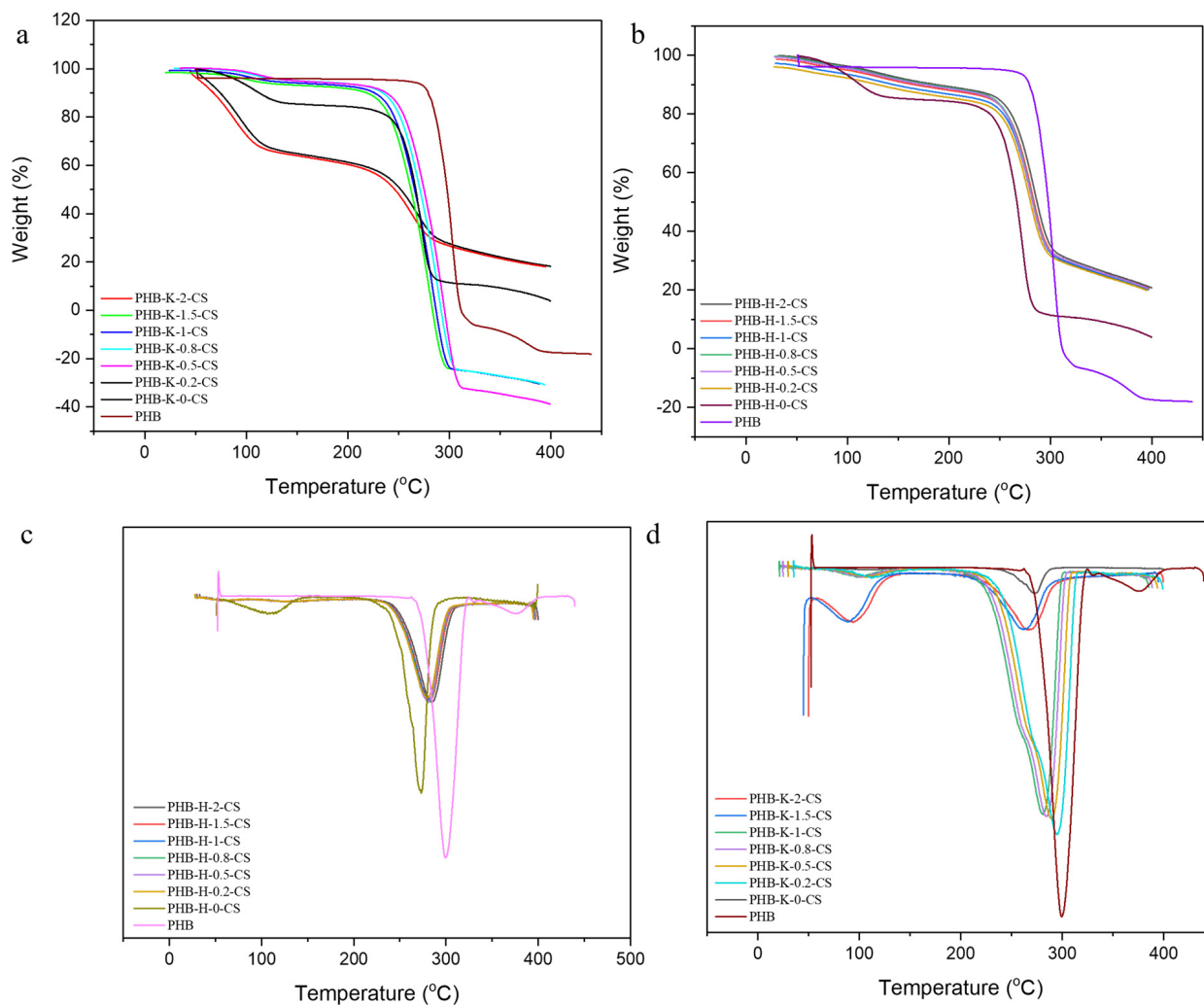**Figure 5.** (**a**) TGA for KOH−treated PHB electrospun nanofibers with 2, 1.5, 1, 0.8, 0.5, and 0.2 *w/v*% CS. (**b**) TGA for H_2O_2−treated PHB electrospun nanofibers with 2, 1.5, 1, 0.8, 0.5, and 0.2 *w/v*% CS (**c**) DTA for H_2O_2−treated PHB electrospun nanofibers with 2, 1.5, 1, 0.8, 0.5, and 0.2 *w/v*% CS. (**d**) DTA for KOH−treated PHB electrospun nanofibers with 2, 1.5, 1, 0.8, 0.5, and 0.2 *w/v*% CS.

After adding different concentrations of CS, the T_1 temperature values of both the KOH and H_2O_2-treated PHB samples are demonstrated in Table 2. We found that the KOH-treated PHB remained in the temperature range of 92.9 °C to 102.4 °C and, the H_2O_2-treated PHB ranged from 110 °C to 128.7 °C among the concentration of CS from 0 to 2 *w/v*%. For the T_2 temperature, the KOH-treated PHB remained within the temperature range of 280–290 °C between 0 and 1 *w/v*% CS and dropped to 268.5 °C at 2 *w/v*% CS. For the H_2O_2-treated PHB, T_2 showed less variation across different concentrations of CS (274.6 °C to 284.4 °C). The T_1 temperature has been attributed to the evaporation of water and acetic acid, which highly depend on the binding contents of the CS on the PHB fibers. This further indicated that KOH-treated PHB fibers could bind more CS than H_2O_2-treated PHB. However, the T_2 degradation temperature suggested that the KOH-treated crystallinity phase was lower than H_2O_2. This is because the addition of chitosan can potentially decrease the thermal stability of PHB as the concentration increases. This has been proven by Rajan's study, where increasing the concentration of CS reduced the thermal stability of the composites [27].

3.4. DSC Analysis of PHB-CS Electrospun Fibers

Tables 5 and 6 show the enthalpies of fusion (H_f) which were the amorphous phase (H_1) and crystallinity phase (H_2), and the crystallinity calculated from the DSC scans using the following equation:

$$\chi = \left(\frac{\Delta H_f}{\Delta H_f^0}\right) \times \frac{100}{w} \tag{1}$$

where ΔH_f is the composite's fusion enthalpy, ΔH_f^0 is the fusion enthalpy of 100% crystalline PHB, and w is the mass fraction of PHB in the composite. The PHB's ΔH_f^0 was calculated to be 146 J/g [28]. As shown in Figure 6, one of the factors lowering the melting temperature in the polymer blend with a crystallizable component was the miscibility of the constituents in the amorphous phase. In this case, the enthalpy fusion of the crystallinity phase (H_2) of both the KOH and H_2O_2-treated PHB-GA-DA-CS electrospun samples showed decreases from 95.3 J/g to 32.8 J/g and from 117.9 J/g to 58.7 J/g, respectively, from 0 to 2 w/v% CS contents, whereas the amorphous phase (H_1) showed mild variations between 3.9 and 7.2 J/g. This is because the presence of highly rigid chitosan molecules surrounding PHB molecules made the PHB molecules in the composites less flexible, inducing less crystallization compared to neat PHB. These changes may be caused by the decrease in PHB lamellar thickness and the percentage of the crystalline phase structure [29]. The crystallinity of PHB is suppressed by the presence of CS in the blend fibers via the chemical interactions between them (hydrogen bonds). These chemical interactions act as a bridge between two polymers, decreasing the crystallinity and aiding the miscibility of the two polymers together. Moreover, the crystallinity of the KOH and H_2O_2-treated PHB-GA-DA-CS electrospun samples showed 45% and 40% reductions, respectively. This is because both KOH and H_2O_2 could cause the de-esterification of PHB and directly, causing the deconstruction of crystallinity structure [30–32]. Moreover, the addition of CS has been reported to cause a reduction in crystallinity after chitosan is added [9]. Additionally, the hydrolysis of PHB due to the KOH treatment could also reduce its lamellar thickness.

Table 5. Enthalpy of fusion and crystallinity of the electrospun PHB-KOH/H_2O_2-treated electrospun nanofibers with 2, 1.5, 1, 0.8, 0.5, and 0.2 w/v% CS.

	Enthalpy of Fusion		Crystallinity
	ΔH_{fusion} (J/g)		%
	H_1	H_2	
PHB-K-0-CS	4.87	95.31	70.40
PHB-K-0.2-CS	3.83	42.60	31.81
PHB-K-0.5-CS	4.03	41.52	31.12
PHB-K-0.8-CS	4.32	38.24	29.14
PHB-K-1-CS	4.34	37.01	28.31
PHB-K-1.5-CS	4.51	35.13	27.12
PHB-K-2-CS	4.52	32.81	25.62

Table 6. Enthalpy of fusion and crystallinity of the electrospun PHB-H_2O_2-treated electrospun nanofibers with 2, 1.5, 1, 0.8, 0.5, and 0.2 w/v% CS.

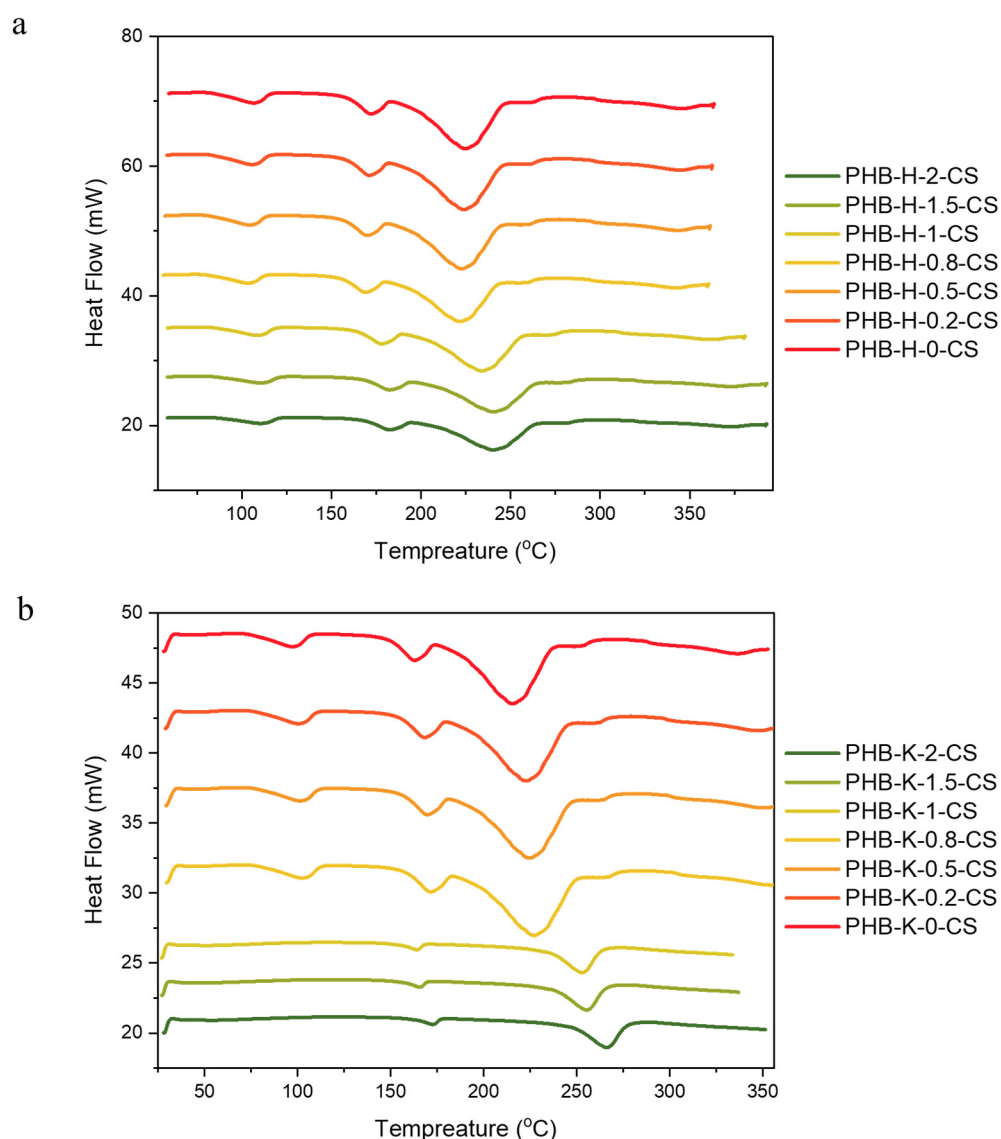|	Enthalpy of Fusion		Crystallinity
Groups	ΔH_{fusion} (J/g)		%
	H_1	H_2	
PHB-H-0-CS	6.80	117.92	85.21
PHB-H-0.2-CS	5.91	72.31	53.62
PHB-H-0.5-CS	6.27	71.23	53.13
PHB-H-0.8-CS	7.02	70.82	53.32
PHB-H-1-CS	7.16	65.21	49.63
PHB-H-1.5-CS	7.19	62.82	47.91
PHB-H-2-CS	7.39	58.73	45.34

Figure 6. DSC analysis of PHB-KOH/H_2O_2-treated electrospun nanofibers with chitosan concentrations of 2, 1.5, 1, 0.8, 0.5, and 0.2 *w/v*%: (**a**) KOH-treated samples and (**b**) H_2O_2-treated samples.

3.5. Hydrophilicity Analysis of PHB-CS Electrospun Fibers with Contact Angle Measurements

Figure 7 illustrates the hydrophilic properties of ten PHB membrane groups at different stages of functionalization. A notably higher water contact angle (WCA) of $95 \pm 7.2°$ was exhibited by the non-treated PHB electrospun membrane compared to the modified one, reflecting its relatively hydrophobicity. However, the KOH and H_2O_2 treatments, which fostered the formation of surface hydroxyl groups, substantially decreased the WCAs to $0 \pm 1.2°$ and $10 \pm 2.2°$, respectively. Upon the deposition of dopamine (DA) onto the PHB membranes, there was a significant increase in the WCAs of both the KOH- and H_2O_2-treated PHB samples to $35 \pm 5.3°$. The inherent hydrophobic properties of the electrospun PHB fibers were initially observed before the post-treatment. However, following the application of a dopamine coating, the PHB fiber membranes underwent a transformation towards increased hydrophilicity [21,22]. Furthermore, when comparing the reduction in the fiber diameter of the PHB after treatment with KOH and H_2O_2, as demonstrated in Table 1, it is evident that the increase in the surface roughness also contributed to enhanced surface hydrophilicity [15,17,21]. Despite an increase in hydrophilicity, the dopamine-coated membranes retained their improved hydrophilicity compared to the untreated PHB membranes, even after undergoing various treatments. The introduction of glutaraldehyde

(GA) and chitosan (CS) further improved the membranes' hydrophilic nature, as evidenced by a minor decrease in the WCA values to approximately 32°. This trend is consistent with early studies [13,33]. Incorporating CS into the PHB membranes lowered the WCA to $20 \pm 4.1°$ and $35 \pm 3.1°$ for the KOH and H_2O_2-treated PHB samples, respectively. Decreases in the WCA were observed across various CS concentrations, ranging from 0.2% to 2% *w/v*. Interestingly, the PHB-DA-GA-CS membranes treated with KOH maintained a relatively consistent WCA of $22 \pm 3.2°$, despite increasing CS contents. In contrast, those treated with H_2O_2 displayed slightly higher WCA values. This difference could be attributed to the distinct processes and efficiency of surface oxidation provided by KOH and H_2O_2. KOH promotes a stable hydrolysis reaction on PHB, breaking the ester linkages and creating carboxyl and hydroxyl groups [17,30,32,34,35]. H_2O_2, on the other hand, generates unstable active oxygen species on the PHB surface over time, resulting in less predictable outcomes [17,34].
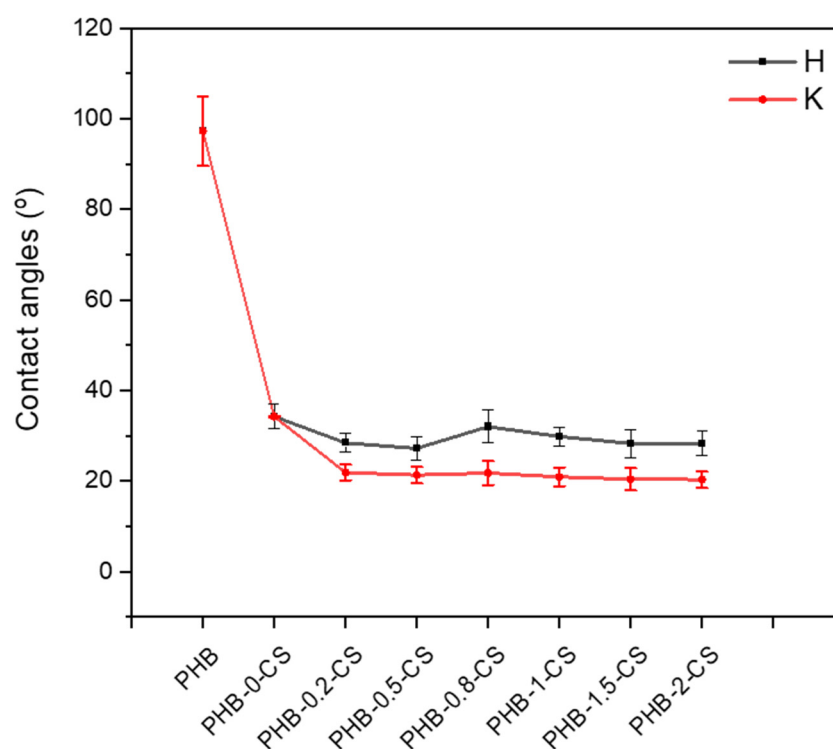

Figure 7. Average water contact angles of the PHB-KOH/H_2O_2-treated electrospun nanofibers with no treatment or treatment with 0, 0.5, 0.8, 1, 1.5, and 2 *w/v*% CS.

3.6. Analysis of Porosity and Specific Surface Area of PHB-CS Electrospun Fibers Using the BET Method

Figure 8 and Tables 7 and 8 display the results of the BET study of the KOH/H_2O_2-treated PHB electrospun nanofibers. Seven fibrous samples were examined for their specific surface area with various CS concentrations. the specific surface area of the KOH-treated PHB electrospun fibers decreased from 338 ± 12.31 m^2/g to 264 ± 12.1 m^2/g, whereas the H_2O_2-treated PHB samples dropped from 338 ± 12.31 m^2/g to 260 ± 11.1 m^2/g. The decrement in the specific surface area with increasing CS concentrations in the PHB matrix can be attributed to a combination of factors, including the chitosan particle size and distribution, viscosity, processing conditions, influence on crystallinity, and crosslinking or physical entanglements [9,36,37]. As chitosan concentration increases, particle agglomeration may lead to a more compact structure, while increased viscosity can result in a more homogeneous and compact structure with fewer voids [14,38]. Additionally, chitosan's potential role as a nucleating agent might promote the formation of denser crystalline regions with reduced surface areas and pore volumes compared to amorphous regions [9]. Furthermore,

crosslinking or physical entanglements induced by chitosan can create a more compact and dense structure, ultimately decreasing the specific surface area and pore volume in the composite material [3,9,39].
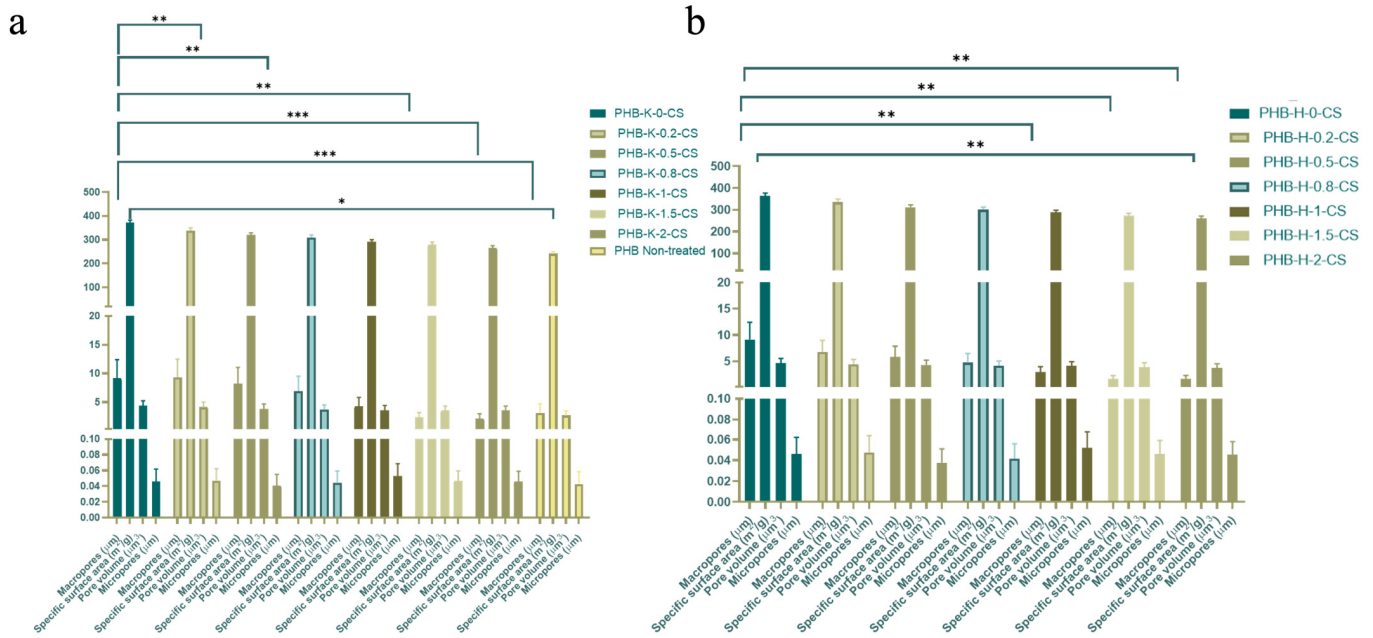

Figure 8. BET analysis of macropore size, micropore size, specific surface area, and pore volume. PHB-KOH/H_2O_2-treated electrospun nanofibers with chitosan concentrations of 2, 1.5, 1, 0.8, 0.5, 0.2, and 0 w/v% are displayed. (**a**) KOH-treated and (**b**) H_2O_2-treated samples. (*** ($p < 0.0001$), ** ($p < 0.0005$), * ($p < 0.001$)).

Table 7. Effects of CS concentration on macropore size, micropore size, specific surface area, and pore volume of PHB-K electrospun membranes.

Groups	Specific Surface Area (m^2/g)
PHB-K-0-CS	371.00 ± 11.30
PHB-K-0.2-CS	338.00 ± 12.30
PHB-K-0.5-CS	319.00 ± 10.20
PHB-K-0.8-CS	309.00 ± 11.20
PHB-K-1-CS	291.00 ± 8.92
PHB-K-1.5-CS	280.00 ± 10.20
PHB-K-2-CS	264.00 ± 12.10
PHB (Non-treated)	276.00 ± 10.20

Table 8. Effect of CS concentration on the specific surface area of PHB-H electrospun membranes.

Groups	Specific Surface Area (m^2/g)
PHB-H-0-CS	371.00 ± 11.30
PHB-H-0.2-CS	338.00 ± 12.30
PHB-H-0.5-CS	319.00 ± 10.20
PHB-H-0.8-CS	309.00 ± 11.20
PHB-H-1-CS	291.00 ± 8.92
PHB-H-1.5-CS	280.00 ± 10.20
PHB-H-2-CS	260.00 ± 11.10

3.7. Stability Assessment of KOH/H₂O₂ PHB-DA-GA-CS Electrospun Samples: UV-Vis and CBR Analytical Techniques

Figure 9 shows the UV-vis analysis of the stability of the KOH/H_2O_2 PHB-DA-GA-CS electrospun samples using CBR analytical techniques. Based on the results shown in Figure 9, the peak intensity between 506 and 550 nm indicated the release of CS. We found that the amounts of CS released from the KOH-treated PHB-DA-GA-CS electrospun fibers were 57.7, 64.0, 84.0, 61.9, 84.3, 89.4 and 103.2% for the membranes loaded with 0, 0.2, 0.5, 0.8, 1, 1.5, or 2 w/v% concentration of CS, while the amounts released from the H_2O_2-treated PHB-DA-GA-CS electrospun fibers were 45.2, 53.8, 65.7, 48.4, 66.5, 69.9 and 80.7% for the membranes loaded with 0, 0.2, 0.5, 0.8, 1, 1.5, to 2 w/v%, respectively. Comparatively, the maximum release of CS from the KOH-treated samples was 23% more than the H_2O_2-treated samples. This is due to the hydrolysis effects of KOH on PHB, which de-esterified its chemical structure. On the other hand, the by-product of PHB remained acidic and caused the CBR to turn red [18,22,33]. The initial slope of the accumulative release profile of CS between the different concentrations represents the rate of CS release from the samples. In general, the KOH-treated PHB-DA-GA-CS electrospun membranes showed a faster release rate than the H_2O_2-treated samples, which has also been reported by other researchers [22,25,33].
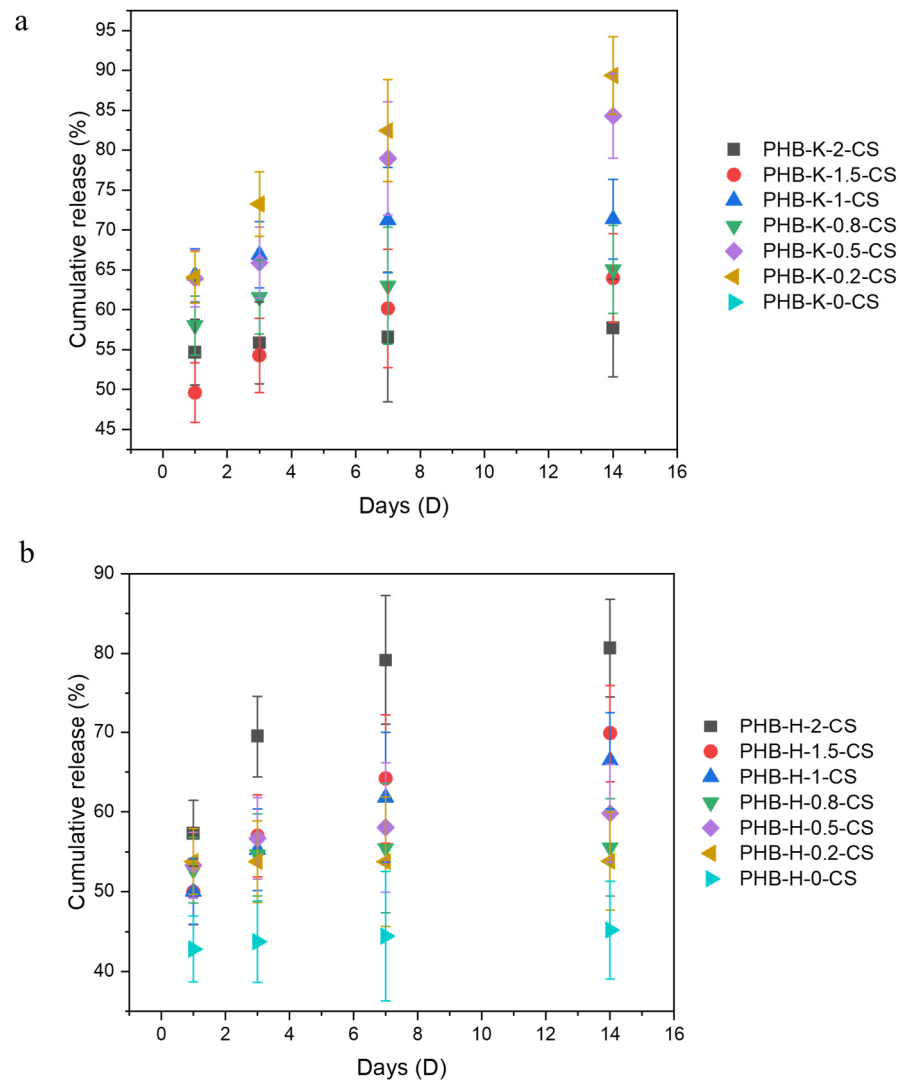

Figure 9. UV-vis of PHB electrospun fibers with (**a**) KOH and (**b**) H_2O_2 treatments with 2, 1.5, 1, 0.8, 0.5, 0.2, and 0 w/v% CS.

3.8. Mechanical Properties of KOH- and H₂O₂-Treated PHB Electrospun Nanofibers with Varying CS Concentrations: Tensile Strength, Toughness, Young's Modulus, and Elongation at Break

The tensile strength, toughness, Young's modulus, and elongation at break of the KOH- and H_2O_2-treated PHB electrospun nanofibers with 0, 0.2, 0.5, 0.8, 1, 1.5, and 2 *w/v*% CS concentrations are presented in Table 9. The CS coating on PHB fibers resulted in enhanced flexibility and reduced stiffness, as evidenced by a decrease in the Young's modulus with increasing CS contents. Notably, the PHB-DA-GA-CS fibers with a 2 *w/v*% CS content exhibited the most significant reduction in Young's modulus, indicating a higher flexibility. Additionally, an inverse correlation was observed between the CS content and elongation at the break of the fibers. Increased CS content led to higher elongation values, indicating improved ductility and resistance to breakage. This behavior aligns with the successful coating of PHB fibers by CS, effectively mitigating their inherent brittleness. Considering the thermal properties analyzed using TGA (Figure 5 and Table 3), the CS-coated PHB fibers demonstrated improved thermal stability compared to the uncoated fibers. This enhanced thermal stability potentially contributed to the observed improvements in the mechanical properties of the CS-coated fibers.

Table 9. Mechanical properties of PHB-KOH-treated electrospun nanofibers with 2, 1.5, 1, 0.8, 0.5, 0.2, and 0 *w/v*% CS.

Groups	Elongation at Break (%)	Young's Modulus (MPa)	Toughness (MPa)	Ultimate Tensile Stress (UTS) (MPa)
PHB-K-0-CS	390	0.00043	56	0.18
PHB-K-0.2-CS	600	0.00044	180	0.6
PHB-K-0.5-CS	490	0.0005	140	0.58
PHB-K-0.8-CS	360	0.00069	89	0.49
PHB-K-1-CS	340	0.001	93	0.56
PHB-K-1.5-CS	330	0.0013	120	0.55
PHB-K-2-CS	250	0.0014	75	0.59

Table 9 and Figure 10 reveal that the hydrolysis effect of KOH on PHB results in relatively lower ultimate tensile stress (UTS) values for the KOH-treated PHB fibers (ranging from 0.59 MPa to 0.18 MPa) compared to the H_2O_2-treated fibers (ranging from 0.77 MPa to 0.43 MPa) as the CS concentrations increased from 0 to 2 *w/v*%. Intriguingly, negligible variations in UTS were observed between the 0 and 1.5 *w/v*% CS concentrations for both the KOH and H_2O_2-treated fibers. However, a 69.4% and 35% reduction in UTS occurred when shifting from 1.5 *w/v*% to 2 *w/v*% CS content in the KOH and H_2O_2-treated fibers, respectively (0.60 MPa to 0.18 MPa and 0.66 MPa to 0.43 MPa). This suggests that the 2 *w/v*% CS concentration has reached the miscibility limit between PHB and CS, leading to phase separation in the blended systems.

Similar to UTS, Figure 10 also shows that the toughness trends for both the KOH and H_2O_2-treated fibers increased with CS concentrations between 0 and 1.5 *w/v*%. After adding 2 *w/v*% CS, a more significant drop in the toughness was observed for the KOH-treated fibers compared to the H_2O_2-treated fibers. Additionally, increasing CS concentrations generally led to higher elongation-at-break values for both the KOH and H_2O_2-treated fibers. The crack-pinning mechanism of CS was likely responsible for the enhanced toughness observed in the blended films. The combination of PHB and CS loading improved the electrospun membrane's resilience due to van der Waals forces, delaying crack propagation. The decreased crystallinity of the KOH-treated PHB, coupled with high CS concentrations, resulted in enhanced miscibility with CS. Moreover, the low toughness of CS may replace PHB as the mechanically dominant material, affecting the mechanical properties of the entire electrospun membrane and leading to a substantial decrease in the toughness of the PHB electrospun samples.
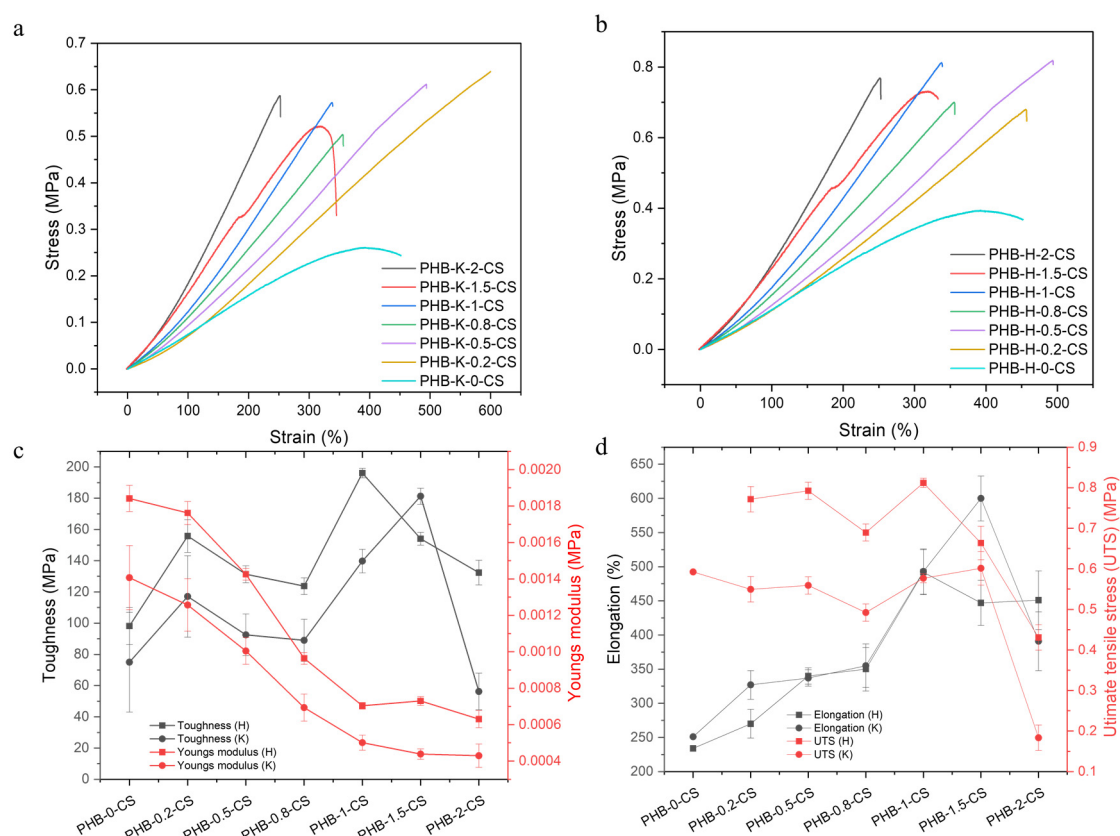
Figure 10. Mechanical properties of PHB electrospun fibers with chitosan concentrations of 2, 1.5, 1, 0.8, 0.5, 0.2, and 0 $w/v\%$: (**a**) Tensile properties of the KOH-treated samples, (**b**) tensile properties of the H_2O_2-treated samples, (**c**) toughness and Young's modulus for both KOH and H_2O_2 treated samples, and (**d**) elongation and ultimate tensile strength (UTS) for both the KOH and H_2O_2 treated samples.

The tensile strength, toughness, Young's modulus, and elongation at break of the PHB-KOH/H_2O_2-treated electrospun nanofibers with 2, 1.5, 1, 0.8, 0.5, 0.2, and 0 $w/v\%$ CS are shown in Tables 9 and 10. The hydrolysis impact of KOH on PHB resulted in relatively smaller values of UTS between KOH (between 0.59 MPa and 0.18 MPa) and H_2O_2-treated PHB electrospun membranes (between 0.77 MPa and 0.43 MPa) with increasing CS concentrations from 0 $w/v\%$ to 2 $w/v\%$. Interestingly, the UTS of both the KOH and H_2O_2-treated electrospun membranes revealed negligible variations between each concentration between 0 and 1.5 $w/v\%$ CS; nevertheless, a 69.4% and 35% reduction in UTS occurred when shifting from 1.5 $w/v\%$ to 2 $w/v\%$ CS content in the KOH and H_2O_2-treated PHB electrospun membranes, respectively (0.60 MPa to 0.18 MPa and 0.66 MPa to 0.43078 MPa). This can be explained by 2 $w/v\%$ CS reaching the limits of miscibility between PHB and CS, which will further induce the phase separation between PHB and CS in blended systems [9]. Similar to UTS, the trend toughness for both KOH and H_2O_2-treated PHB electrospun membranes increased when the concentration of CS applied was between 0 $w/v\%$ and 1.5 $w/v\%$. After 2 $w/v\%$ CS was added, the KOH-treated PHB electrospun membranes, as opposed to the H_2O_2-treated membranes, demonstrated a more notable drop in toughness. Additionally, after a high concentration of CS was applied, the elongation-at-break of the PHB electrospun membranes that had been treated with KOH or H_2O_2 showed generally increasing trends. The impacts of CS, which toughen materials through a crack-pinning mechanism, may be responsible for the rise in blended films [26]. The electrospun membranes become more resilient when PHB is combined with CS loading due to the van der Waals force of attraction between them, which also delays the spread of cracks. When a high concentration of CS was introduced, the reduced crystallinity of the KOH-treated PHB causes increased miscibility with CS. Furthermore, the

low toughness of CS may have caused the PHB to be replaced as a mechanical-dominated material, affecting the mechanical characteristics of entire electrospun membranes and resulting in a considerable decrease in the toughness of the PHB electrospun samples.

Table 10. Mechanical properties of PHB-H_2O_2 treated electrospun nanofibers with 2, 1.5, 1, 0.8, 0.5, 0.2, and 0 w/v% CS.

Groups	Elongation at Break (%)	Young's Modulus (MPa)	Toughness (MPa)	Ultimate Tensile Stress (UTS) (MPa)
PHB-H-0-CS	450	0.00063	130	0.43
PHB-H-0.2-CS	450	0.00073	150	0.66
PHB-H-0.5-CS	490	0.0007	200	0.81
PHB-H-0.8-CS	350	0.00096	120	0.69
PHB-H-1-CS	340	0.0014	130	0.79
PHB-H-1.5-CS	270	0.0018	160	0.77
PHB-H-2-CS	230	0.0018	98	0.77

4. Conclusions

In this study, KOH and H_2O_2 pre-treatments were found to be very effective in affecting the surface morphology, thermal and structural stability, and mechanical properties of PHB nanofibers. The fiber morphology and porous structure changed noticeably. CS was successfully coated onto the PHB nanofibers, which improved the hydrophilicity of the nanofibers. CS coating of PHB nanofibers led to remarkable improvements in their mechanical properties and a reduction in their brittleness. However, beyond a threshold concentration of 2 w/v% of CS, it had a detrimental impact on the mechanical properties. As CS began to dominate the mechanical behavior, the tensile strength and toughness experienced a significant decrease. Thermal stability analyses demonstrated an overall enhancement in its resistance to degradation, which was particularly noticeable with the KOH pre-treatment. Our findings have highlighted the crucial balance needed when utilizing CS concentrations to achieve a desirable combination of mechanical, thermal, and morphological properties. Despite these encouraging results, future work should investigate the cellular responses to these enhanced nanofibers through in vitro and in vivo trials to confirm their suitability in regenerative medicine.

Author Contributions: Conceptualization, Y.Z. and F.Z.; methodology, Y.Z. and F.Z.; software, Y.Z. and F.Z.; validation, Y.Z., D.L., X.L., Y.L., B.L. and F.Z.; formal analysis, Y.Z. and F.Z.; investigation, Y.Z. and F.Z.; resources, Y.Z., D.L., Y.L., B.L. and F.Z.; data curation, Y.Z. and X.L.; writing—original draft preparation, Y.Z., B.L. and F.Z.; writing—review and editing, Y.Z., D.L., X.L., Y.L., B.L. and F.Z.; visualization, Y.Z.; supervision, D.L., Y.L., B.L. and F.Z.; project administration, Y.Z., D.L., Y.L., B.L. and F.Z.; funding acquisition, B.L. All authors have read and agreed to the published version of the manuscript.

Data Availability Statement: The data presented in this study are available on request from the corresponding author.

Conflicts of Interest: The authors declare no conflict of interest.

References

1. Sasidharan, R.S.; Bhat, S.G.; Chandrasekaran, M. Biocompatible polyhydroxybutyrate (PHB) production by marine Vibrio azureus BTKB33 under submerged fermentation. *Ann. Microbiol.* **2014**, *65*, 455–465. [CrossRef]
2. Mohammadalipour, M.; Karbasi, S.; Behzad, T.; Mohammadalipour, Z.; Zamani, M. Effect of cellulose nanofibers on polyhydroxybutyrate electrospun scaffold for bone tissue engineering applications. *Int. J. Biol. Macromol.* **2022**, *220*, 1402–1414. [CrossRef] [PubMed]

3. Demcisakova, Z.; Luptakova, L.; Tirpakova, Z.; Kvasilova, A.; Medvecky, L.; De Spiegelaere, W.; Petrovova, E. Evaluation of Angiogenesis in an Acellular Porous Biomaterial Based on Polyhydroxybutyrate and Chitosan Using the Chicken Ex Ovo Chorioallantoic Membrane Model. *Cancers* **2022**, *14*, 4194. [CrossRef] [PubMed]
4. Movahedi, M.; Karbasi, S. Electrospun halloysite nanotube loaded polyhydroxybutyrate-starch fibers for cartilage tissue engineering. *Int. J. Biol. Macromol.* **2022**, *214*, 301–311. [CrossRef]
5. Lezcano, M.F.; Álvarez, G.; Chuhuaicura, P.; Godoy, K.; Alarcón, J.; Acevedo, F.; Gareis, I.; Dias, F.J. Polyhydroxybutyrate (PHB) Scaffolds for Peripheral Nerve Regeneration: A Systematic Review of Animal Models. *Biology* **2022**, *11*, 706. [CrossRef]
6. Guo, W.; Yang, K.; Qin, X.; Luo, R.; Wang, H.; Huang, R. Polyhydroxyalkanoates in tissue repair and regeneration. *Eng. Regen.* **2022**, *3*, 24–40. [CrossRef]
7. Trujillo-Miranda, M.; Apsite, I.; Agudo, J.A.R.; Constante, G.; Ionov, L. 4D Biofabrication of Mechanically Stable Tubular Constructs Using Shape Morphing Porous Bilayers for Vascularization Application. *Macromol. Biosci.* **2022**, *23*, e2200320. [CrossRef]
8. Hetemi, D.; Pinson, J. Surface functionalisation of polymers. *Chem. Soc. Rev.* **2017**, *46*, 5701–5713. [CrossRef]
9. Zhou, Y.; Li, Y.; Li, D.; Yin, Y.; Zhou, F. Electrospun PHB/Chitosan Composite Fibrous Membrane and Its Degradation Behaviours in Different pH Conditions. *J. Funct. Biomater.* **2022**, *13*, 58. [CrossRef]
10. Li, J.; Liu, Y.; Abdelhakim, H.E. Drug Delivery Applications of Coaxial Electrospun Nanofibres in Cancer Therapy. *Molecules* **2022**, *27*, 1803. [CrossRef]
11. Righetti, M.C.; Cinelli, P.; Aliotta, L.; Bianchi, E.; Tricoli, F.; Seggiani, M.; Lazzeri, A. Immiscible PHB/PB S and PHB/PBSA blends: Morphology, phase composition and modelling of elastic modulus. *Polym. Int.* **2022**, *71*, 47–56. [CrossRef]
12. Notario-Pérez, F.; Martín-Illana, A.; Cazorla-Luna, R.; Ruiz-Caro, R.; Veiga, M.D. Applications of Chitosan in Surgical and Post-Surgical Materials. *Mar. Drugs* **2022**, *20*, 396. [CrossRef] [PubMed]
13. Kang, J.; Yun, S.I. Chitosan-reinforced PHB hydrogel and aerogel monoliths fabricated by phase separation with the solvent-exchange method. *Carbohydr. Polym.* **2022**, *284*, 119184. [CrossRef] [PubMed]
14. Seddighian, A.; Ganji, F.; Baghaban-Eslaminejad, M.; Bagheri, F. Electrospun PCL scaffold modified with chitosan nanoparticles for enhanced bone regeneration. *Prog. Biomater.* **2021**, *10*, 65–76. [CrossRef]
15. Liu, Z.; Wei, W.; Tremblay, P.L.; Zhang, T. Electrostimulation of fibroblast proliferation by an electrospun poly (lactide-co-glycolide)/polydopamine/chitosan membrane in a humid environment. *Colloids Surf. B Biointerfaces* **2022**, *220*, 112902. [CrossRef]
16. Arulselvan, P.; Fard, M.T.; Tan, W.S.; Gothai, S.; Fakurazi, S.; Norhaizan, M.E.; Kumar, S.S. Role of Antioxidants and Natural Products in Inflammation. *Oxid. Med. Cell. Longev.* **2016**, *2016*, 5276130. [CrossRef]
17. Yang, X.; Zhao, K.; Chen, G.-Q. Effect of surface treatment on the biocompatibility of microbial polyhydroxyalkanoates. *Biomaterials* **2001**, *23*, 1391–1397. [CrossRef]
18. Jiang, Y.; Mikova, G.; Kleerebezem, R.; van der Wielen, L.A.; Cuellar, M.C. Feasibility study of an alkaline-based chemical treatment for the purification of polyhydroxybutyrate produced by a mixed enriched culture. *AMB Express* **2015**, *5*, 5. [CrossRef]
19. Rouxhet, L.; Duhoux, F.; Borecky, O.; Legras, R.; Schneider, Y.J. Adsorption of albumin, collagen, and fibronectin on the surface of poly (hydroxybutyrate-hydroxyvalerate) (PHB/HV) and of poly (ε-caprolactone) (PCL) films modified by an alkaline hydrolysis and of poly (ethylene terephtalate) (PET) track-etched membranes. *J. Biomater. Sci. Polym. Ed.* **1998**, *9*, 1279–1304. [CrossRef]
20. Zou, Y.; Yang, M.; Tao, Q.; Zhu, K.; Liu, X.; Wan, C.; Harder, M.K.; Yan, Q.; Liang, B.; Ntaikou, I.; et al. Recovery of polyhydrox-yalkanoates (PHAs) polymers from a mixed microbial culture through combined ultrasonic disruption and alkaline digestion. *J. Environ. Manag.* **2023**, *326*, 116786. [CrossRef]
21. Charpentier, P.A.; Maguire, A.; Wan, W.-K. Surface modification of polyester to produce a bacterial cellulose-based vascular prosthetic device. *Appl. Surf. Sci.* **2006**, *252*, 6360–6367. [CrossRef]
22. Ke, Y.; Liu, C.; Zhang, X.; Xiao, M.; Wu, G. Surface Modification of Polyhydroxyalkanoates toward Enhancing Cell Compatibility and Antibacterial Activity. *Macromol. Mater. Eng.* **2017**, *302*, 1700258. [CrossRef]
23. Morshed, M.N.; Behary, N.; Bouazizi, N.; Guan, J.; Chen, G.; Nierstrasz, V. Surface modification of polyester fabric using plasma-dendrimer for robust immobilization of glucose oxidase enzyme. *Sci. Rep.* **2019**, *9*, 15730. [CrossRef]
24. Park, J.S.; Kim, J.-M.; Lee, S.J.; Lee, S.G.; Jeong, Y.-K.; Kim, S.E.; Lee, S.C. Surface hydrolysis of fibrous poly(ε-caprolactone) scaffolds for enhanced osteoblast adhesion and proliferation. *Macromol. Res.* **2007**, *15*, 424–429. [CrossRef]
25. Choong, C.; Yuan, S.; Thian, E.S.; Oyane, A.; Triffitt, J. Optimization of poly(ε-caprolactone) surface properties for apatite formation and improved osteogenic stimulation. *J. Biomed. Mater. Res. Part A* **2012**, *100A*, 353–361. [CrossRef]
26. Chong, M.S.K.; Teoh, S.-H.; Teo, E.Y.; Zhang, Z.-Y.; Lee, C.N.; Koh, S.; Choolani, M.; Chan, J. Beyond Cell Capture: Antibody Conjugation Improves Hemocompatibility for Vascular Tissue Engineering Applications. *Tissue Eng. Part A* **2010**, *16*, 2485–2495. [CrossRef]
27. Rajan, R.; Sreekumar, P.A.; Joseph, K.; Skrifvars, M. Thermal and mechanical properties of chitosan reinforced polyhydroxybu-tyrate composites. *J. Appl. Polym. Sci.* **2012**, *124*, 3357–3362. [CrossRef]
28. Young, R.; Terenghi, G.; Wiberg, M. Poly-3-hydroxybutyrate (PHB): A resorbable conduit for long-gap repair in peripheral nerves. *Br. J. Plast. Surg.* **2002**, *55*, 235–240. [CrossRef]
29. Ikejima, T.; Inoue, Y. Crystallization behavior and environmental biodegradability of the blend films of poly(3-hydroxybutyric acid) with chitin and chitosan. *Carbohydr. Polym.* **2000**, *41*, 351–356. [CrossRef]

30. Kühn, S.; van Werven, B.; van Oyen, A.; Meijboom, A.; Rebolledo, E.L.B.; van Franeker, J.A. The use of potassium hydroxide (KOH) solution as a suitable approach to isolate plastics ingested by marine organisms. *Mar. Pollut. Bull.* **2017**, *115*, 86–90. [CrossRef]
31. Mothes, G.; Schnorpfeil, C.; Ackermann, J.-U. Production of PHB from Crude Glycerol. *Eng. Life Sci.* **2007**, *7*, 475–479. [CrossRef]
32. Yeo, J.C.C.; Lin, T.T.; Koh, J.J.; Low, L.W.; Tan, B.H.; Li, Z.; He, C. Insights into the nucleation and crystallization analysis of PHB-rubber toughened PLA biocomposites. *Compos. Commun.* **2021**, *27*, 100894. [CrossRef]
33. Saratale, G.D.; Oh, M.-K. Characterization of poly-3-hydroxybutyrate (PHB) produced from Ralstonia eutropha using an alkali-pretreated biomass feedstock. *Int. J. Biol. Macromol.* **2015**, *80*, 627–635. [CrossRef] [PubMed]
34. Schaub, N.J.; Le Beux, C.; Miao, J.; Linhardt, R.J.; Alauzun, J.G.; Laurencin, D.; Gilbert, R.J. The Effect of Surface Modification of Aligned Poly-L-Lactic Acid Electrospun Fibers on Fiber Degradation and Neurite Extension. *PLoS ONE* **2015**, *10*, e0136780. [CrossRef] [PubMed]
35. Kumar, S.; Koh, J. Physiochemical, Optical and Biological Activity of Chitosan-Chromone Derivative for Biomedical Applications. *Int. J. Mol. Sci.* **2012**, *13*, 6102–6116. [CrossRef] [PubMed]
36. Desai, K.G.H.; Park, H.J. Preparation and characterization of drug-loaded chitosan-tripolyphosphate microspheres by spray drying. *Drug Dev. Res.* **2005**, *64*, 114–128. [CrossRef]
37. Foroughi, M.R.; Karbasi, S.; Khoroushi, M.; Khademi, A.A. Polyhydroxybutyrate/chitosan/bioglass nanocomposite as a novel electrospun scaffold: Fabrication and characterization. *J. Porous Mater.* **2017**, *24*, 1447–1460. [CrossRef]
38. Yang, Y.; Gu, X.; Tan, R.; Hu, W.; Wang, X.; Zhang, P.; Zhang, T. Fabrication and properties of a porous chitin/chitosan conduit for nerve regeneration. *Biotechnol. Lett.* **2004**, *26*, 1793–1797. [CrossRef]
39. Karbasi, S.; Alizadeh, Z.M. Effects of multi-wall carbon nanotubes on structural and mechanical properties of poly(3-hydroxybutyrate)/chitosan electrospun scaffolds for cartilage tissue engineering. *Bull. Mater. Sci.* **2017**, *40*, 1247–1253. [CrossRef]